Published in final edited form as:

Adv Mater. 2018 September ; 30(38): e1802061. doi:10.1002/adma.201802061.

Two-Dimensional Antimonene-Based Photonic Nanomedicine for Cancer Theranostics

Wei Tao,
Center for Nanomedicine, Brigham and Women's Hospital, Harvard Medical School, Boston, MA 02115, USA

Xiaoyuan Ji,
Center for Nanomedicine, Brigham and Women's Hospital, Harvard Medical School, Boston, MA 02115, USA

School of Pharmaceutical Sciences (Shenzhen), Sun Yat-sen University, Guangzhou 510275, China

Xianbing Zhu,
School of Life Sciences, Tsinghua University Beijing 100084, China

Li Li,
Wellman Center for Photomedicine, Massachusetts General Hospital, Harvard Medical School, Boston, MA 02114, USA

Junqing Wang,
Center for Nanomedicine, Brigham and Women's Hospital, Harvard Medical School, Boston, MA 02115, USA

Ye Zhang,
Center for Nanomedicine, Brigham and Women's Hospital, Harvard Medical School, Boston, MA 02115, USA

Phei Er Saw,
Center for Nanomedicine, Brigham and Women's Hospital, Harvard Medical School, Boston, MA 02115, USA

Wenliang Li,
Center for Nanomedicine, Brigham and Women's Hospital, Harvard Medical School, Boston, MA 02115, USA

Na Kong,
Center for Nanomedicine, Brigham and Women's Hospital, Harvard Medical School, Boston, MA 02115, USA

ofarokhzad@bwh.harvard.edu.
[+]Present address: School of Pharmaceutical Sciences (Shenzhen), Sun Yat-sen University, Guangzhou 510275, China

Supporting Information
Supporting Information is available from the Wiley Online Library or from the author.

Conflict of Interest
O.C.F. declares financial interests in Seer Biosciences, Selecta Biosciences, Tarveda Therapeutics, and Placon Therapeutics.

Sir Run Run Shaw Hospital, Zhejiang University School of Medicine, Hangzhou, Zhejiang 310000, China

Mohammad Ariful Islam,
Center for Nanomedicine, Brigham and Women's Hospital, Harvard Medical School, Boston, MA 02115, USA

Tian Gan,
Center for Nanomedicine, Brigham and Women's Hospital, Harvard Medical School, Boston, MA 02115, USA

Xiaowei Zeng[+],
School of Life Sciences, Tsinghua University Beijing 100084, China

Han Zhang,
Shenzhen Engineering Laboratory of Phosphorene and Optoelectronics SZU–NUS Collaborative Innovation Center for Optoelectronic Science and Technology, and Key Laboratory of Optoelectronic Devices and Systems of Ministry of Education and Guangdong Province Shenzhen University, Shenzhen 518060, China

Morteza Mahmoudi,
Center for Nanomedicine, Brigham and Women's Hospital, Harvard Medical School, Boston, MA 02115, USA

Guillermo J. Tearney,
Wellman Center for Photomedicine, Massachusetts General Hospital, Harvard Medical School, Boston, MA 02114, USA

Omid C. Farokhzad
Center for Nanomedicine, Brigham and Women's Hospital, Harvard Medical School, Boston, MA 02115, USA

Abstract

Antimonene (AM) is a recently described two-dimensional (2D) elemental layered material. In this study, a novel photonic drug-delivery platform based on 2D PEGylated AM nanosheets (NSs) is developed. The platform's multiple advantages include: i) excellent photothermal properties, ii) high drug-loading capacity, iii) spatiotemporally controlled drug release triggered by near-infrared (NIR) light and moderate acidic pH, iv) superior accumulation at tumor sites, v) deep tumor penetration by both extrinsic stimuli (i.e., NIR light) and intrinsic stimuli (i.e., pH), vi) excellent multimodal-imaging properties, and vii) significant inhibition of tumor growth with no observable side effects and potential degradability, thus addressing several key limitations of cancer nanomedicines. The intracellular fate of the prepared NSs is also revealed for the first time, providing deep insights that improve cellular-level understanding of the nano–bio interactions of AM-based NSs and other emerging 2D nanomaterials. To the best of knowledge, this is the first report on 2D AM-based photonic drug-delivery platforms, possibly marking an exciting jumping-off point for research into the application of 2D AM nanomaterials in cancer theranostics.

Keywords

antimonene; cancer theranostics; drug delivery; nanomedicine; two-dimensional nanosheets

Owing to the extraordinary success of graphene,[1] two-dimensional (2D) nanomaterials have now attracted extensive interest to become one of the most active research areas within the field of nanotechnology.[2] With fascinating physical and chemical properties, 2D nanomaterials have many promising applications in areas such as electronics,[3] optoelectronics,[4] water sterilization,[5] catalysis,[6] biomedicine,[7] and energy storage and conversion.[8] Despite their scarcity, elemental 2D nanomaterials are of particular interest, as they are the most chemically tractable for synthetic exploration.[9] In addition to graphene, other examples include borophene (group 13, boron group),[10] silicene and germanene (group 14, the carbon group),[11] and black phosphorus (BP, group 15, the nitrogen group).[12] In recent years, another 2D nanomaterial composed of a group-15 element, antimonene (hereinafter AM), was predicted via first-principle calculations.[13] Theoretically, AM has excellent thermal conductivity,[14] superior carrier mobility, good stability, strain-induced band transition,[13] and extraordinary spintronic properties.[15] All these factors imply that AM might have more-promising properties and applications than graphene, transition-metal dichalcogenides (TMDs, e.g., MoS_2, $MoSe_2$, WS_2, and WSe_2), or BP.[13,16] Very recently, experimentally synthesized AM was obtained through mechanical isolation or liquid-phase exfoliation.[16] Our latest study also demonstrated the excellent near-infrared (NIR) optical properties of AM quantum dots (AMQDs) and their promising application as photothermal agents.[17] Despite the rapid progress implied by the work mentioned above, the experimental study of 2D AM remains largely unexplored, especially in biomedicine.

Graphene, TMDs, and BP have all shown exciting potential when developed as nanomedicines for theranostic applications.[7,18] Considering the similarities in both morphology and function between these 2D nanomaterials and AM,[13,16] their successful application will greatly encourage the exploration of AM's usefulness in biomedicine. Different from our previously reported ultrasmall AMQDs, nanosheet (NS)-shaped AM will have a ultrahigh surface-to-volume ratio,[19] which will lead to extensive surface interactions with theranostic molecules [e.g., doxorubicin (DOX) and Cy 5.5] and generate a high loading capacity of these molecules. Such ultrathin 2D structure may also enable rapid responses to external stimuli that have proven utility in triggered/controlled release of loaded molecules (i.e., multiresponsive drug release). Moreover, AM-based nanomedicines might hold even greater promise as cancer theranostics. For example, AM-based nanomaterials have demonstrated superior physicochemical properties (e.g., mechanical stability and chemically tractability) compared with other 2D materials,[9,16,20] including BP and MoS_2. Notably, antimonial drugs have been in clinical use for several centuries,[21] which might signal that AM-based nanomedicines may hold more promise than the more-extensively studied graphene, TMDs, and BP. Therefore, the development of NS-shaped AM photonic drug-delivery platforms for cancer theranostics is especially exciting.

Herein, we designed an NS-shaped AM-based nanomedicine for multimodal-imaging-guided cancer theranostics (Scheme 1): i) we systematically studied the biocompatibility,

degradability, and performance of the NSs as photonic drug-delivery systems, both in vitro and in vivo. At our test dose, PEG-coated AM (AM-PEG) NSs showed an excellent photothermal conversion efficacy of 41.8% and high DOX loading capacity of 150.0%. The prepared photonic AM-PEG/DOX NSs demonstrated excellent multiresponse (i.e., pH and NIR responsive) drug-release capabilities, as well as effective tumor accumulation, and deep tumor penetration of the loaded drugs by both extrinsic stimuli (i.e., NIR light) and intrinsic stimuli (i.e., pH). ii) As thoroughly discussed in several other significant reports,[22] understanding the cellular interactions of nanomaterials is of critical importance for their safe and efficient biomedical application. Therefore, a cellular-level understanding of nano–bio interactions (i.e., intracellular fate) of these emerging 2D nanomaterials is urgently needed. Nevertheless, systematic study of the intracellular mechanisms (e.g., detailed molecular mechanisms and kinetic pathways) of these 2D nanomaterials is still in its infancy. Our study sheds light on the intracellular fate of these AM-based NSs, which is expected to provide deep insights and build a foundation for the emerging field of 2D nanomaterials in cancer theranostics. iii) With excellent multimodal-imaging properties (fluorescence/photoacoustic (PA)/photothermal imaging), the AM-PEG/DOX NSs achieved significant antitumor efficacy both in vitro and in vivo through combined photothermal chemotherapy. Taken together, our findings are the first demonstration of the promise of AM as a superior 2D delivery platform for cancer theranostics and also help reveal the intracellular fate of these AM-based NSs in cancer cells.

In the first set of experiments, we utilized a modified liquid-exfoliation strategy to develop the 2D AM NSs from bulk antimony.[16a,17] Transmission electron microscopy (TEM) and atomic force microscopy (AFM) were used to access the morphology of the prepared AM NSs (Figure S1a–d, Supporting Information). An average size of ≈140 nm of the liquid-exfoliated AM NSs was obtained on the basis of TEM and AFM analysis (thickness of the captured NS: ≈4 nm). The chemical composition of AM NSs was confirmed by X-ray photo-electron spectroscopy (XPS) and scanning transmission electron microscopy (STEM) with energy-dispersive X-ray spectroscopy (EDS). Sb and O were detected in both the XPS survey spectrum and EDS mapping images of AM NSs, indicating the high purity of our final products (Figure S2a,b, Supporting Information). The EDS-elemental distribution showed the presence of O, which was anticipated considering that these NSs were air-dried, also consistent with recent reports.[15b] Moreover, X-ray diffractometry was used to analyze the crystal structure of the prepared AM NSs (Figure S2c, Supporting Information), indexing them as hexagonal antimony (crystal structure of β-phase antimony), which is also consistent with JCPDS No. 35–0732.[15b] Figure S3a in the Supporting Information shows the Raman spectra of bulk antimony and exfoliated several-layer AM NSs, which perfectly match the spectra of bulk antimony,[23] further confirming the predicted β-phase characteristic of AM (Figure S3b,c, Supporting Information).[14] The A_{1g} peak at ≈146 cm $^{-1}$ refers to the out-of-plane vibrational mode, while the E_g peak at ≈108 cm^{-1} is identified as the in-plane vibrational mode, suggesting that the exfoliated AM NSs were structurally no different from their corresponding bulk counterpart. Owing to the sample thickness changes from bulk form to a few nanometers in thickness,[15b] a slight shift was observed compared to bulk antimony, which is quite similar to the Raman shifting seen with thin BP NSs.[24]

DSPE-PEG (18:0 PEG3000) was further introduced to functionalize these NSs via hydrophobic interactions and van der Waals forces to improve their dispersity/stability (Figure S4, Supporting Information), biocompatibility, and tumor targeting.[22a,25] As shown in Figure 1a–d, the average size of AM-PEG NSs was decreased to ≈90 nm (thickness of the captured NS: ≈6 nm), since bath sonication broke down AM NSs during PEGylation.[18a,26] After PEGylation, the density of O (red) colors was much higher than that of AM NSs, and two other elements, C (magenta) and N (yellow), appeared in EDS mapping of AM-PEG NSs (Figure S5a, Supporting Information), indicating the successful surface coating by DSPE-PEG (i.e., extra C, O, and N elements from the surface-coated DSPE-PEG). The PEGylation of AM NSs was further confirmed by Fourier transform infrared (FT-IR) spectra (Figure S5b, Supporting Information). The developed NSs showed superior photothermal effects (Figure S6, Supporting Information), and photothermal conversion efficacy was calculated at 41.8% using previously reported methods.[17] The good in vitro biocompatibility of these NSs is demonstrated and discussed in the Supporting Information.

After fully characterizing the developed AM-based NSs, we continued to explore their potential as robust drug-delivery platforms. 2D nanomaterials such as graphene and their derivatives, with sp^2-bonded carbon surfaces and high surface area, have been widely studied as drug-delivery platforms to interact with various drug molecules through π-π stacking and hydrophobic interactions.[19,27] Considering their similarity with these 2D nanomaterials, there were high expectations regarding the potential loading capacity of AM-based NSs. An AM-PEG NS solution (0.2 mg mL^{-1}) was simply impregnated with various concentrations of DOX (a typical commercial chemotherapy drug) and stirred for 24 h. After the excess free DOX molecules were completely removed, UV–vis–NIR spectra were investigated to calculate the drug-loading capacity of AM-PEG NSs (Figure 1e). As the feeding concentration of DOX increased, the loading content of DOX molecules also increased almost linearly, with the highest drug-loading capacity (weight ratios) reached at our tested conditions being 150.0% (Figure 1f and Figure S7, Supporting Information), significantly higher than a variety of nanoparticle-based delivery platforms with a shared range of ≈10–30% loaded drug molecules.[28] We also found that AM-PEG/DOX NSs with the characteristic color of DOX dispersed well in water without any detectable agglomeration, and the red color remained on the tube wall after centrifugation through becoming attached to the surface of NSs (Figure 1g). The successful loading of DOX onto the surface of AM-PEG NSs was further confirmed by FT-IR spectroscopy (Figure S8a, Supporting Information). Moreover, the fluorescence of DOX molecules loaded on the surface of AM-PEG NSs could be partially quenched, indicating a strong interaction between the AM-PEG NSs and DOX molecules (Figure S8b, Supporting Information).[18a,26] Additionally, the densities of elemental C, O, and N on the surface of these NSs were much higher after DOX loading in the STEM–EDS mapping images (Figure 1h). The loading of the drug molecules onto the surface of AM-based NSs may be attributed to hydrophobic interactions,[26] while the high loading capacity may be explained by the relatively high surface area of these NSs, similar to other typical 2D nanomaterials.[18a,26]

Nano-delivery-platforms responsive to the tumor microenvironment (TME) enable spatiotemporal control of drug release, offering a promising strategy to address the issue of premature drug release during systemic circulation. Therefore, the in vitro release behavior

of DOX molecules from the AM-PEG/DOX NSs was further analyzed under different treatments. As illustrated in Figure 1i, only 7.4% of DOX was released from the NSs at pH 7.4 over a span of 24 h, while 24.0% of DOX was released at pH 5.0 over the same period. This pH-responsive release of drugs will benefit the application of AM-PEG/DOX NSs for cancer therapy, given the acidic nature of the TME. The pH-responsive release could be caused by the protonation of amino groups in DOX molecules under acidic conditions (pH = 5.0), leading to an increase in hydrophilicity and subsequent triggered release of DOX molecules. Moreover, the NIR-responsive release behavior of DOX molecules was also confirmed. The accumulated release of DOX was drastically increased to 45.1% and 69.8% at pH 7.4 and 5.0, respectively, under laser irradiation for 5 min at certain time intervals. These results indicate that NIR-induced local hyperthermia could also act as an on/off stimulus for controlled release of DOX molecules from AM-PEG/DOX NSs. It is particularly worth mention that, although numerous studies have focused on developing stimuli-responsive delivery platforms with a diverse library of responsive materials and a wide range of stimuli, because clinical translation is fraught with serious problems, very few have reached clinical trials.[22a,29] The major reason for this dilemma is the sophisticated chemistry involved in the design of most of the platforms, which complicates their pharmaceutical development and scalability. Thus, simpler design and the use of off-the-shelf biomaterials without major chemical modifications will significantly help their scale-up and translational potential. Moreover, more-precise control could be achieved through the use of extrinsic stimuli such as light, heat, ultra-sound, electric fields, and magnetic field; that is, extrinsic stimuli may increase the potential for clinical translation, which helps explain why stimuli-responsive nanoplatforms that have reached clinical trials or approval were based on extrinsic stimuli (e.g., NanoTherm, MTC-DOX, and ThermoDox).[30] Therefore, encouraged by these exciting results, we have good reason to believe that these AM-PEG/DOX NSs may be a better option for 2D nanomedicines for cancer theranostics, for the following reasons: i) all the components of AM-PEG/DOX NSs are already clinically approved or possess potential for clinical transformation (i.e., antimonials have been utilized in medicine for several centuries,[21a] and both DSPE-PEG and DOX have already been approved by U.S. FDA). ii) They respond to both extrinsic stimuli (i.e., NIR light) and intrinsic stimuli (i.e., pH). iii) Multiresponsive drug release is achieved via a platform of relatively simple design compared with many other nanoplatforms.

In the next set of experiments, we moved on to provide a cellular-level understanding of nano–bio interactions (i.e., intracellular fate) of the developed NSs. After the AM-PEG NSs arrive in the external milieu of tumor cells via the blood circulation, they interact with the plasma membrane surface of cancer cells and become internalized via endocytosis pathways.[22b–d,31] Clathrin-dependent and -independent endocytosis are two major such endocytic pathways. Moreover, clathrin-independent endocytosis encompasses macropinocytosis, caveolin-dependent, and caveolin-independent (RhoA, Cdc42, Arf-6, and Flotillin-dependent) pathways.[32] Since the intracellular fate of AM-PEG NSs is critical to their success, they were labeled with Cy5.5 by conjugating Cy5.5-NHS to DSPE-PEG-NH_2 before being coated onto the surface of these NSs (Figure S9, Supporting Information) and employed to screen all possible endocytosis pathways. MCF-7 were used as model cells. The cellular uptake mechanism of AM-PEG NSs is indeed via an energy-dependent

endocytosis, rather than simple passive diffusion (Figure S10, Supporting Information). After 4 h incubation, MCF-7 cells were treated with antibodies and subjected to immunofluorescence assays. Antibodies included Caveolin, Arf-6, Clathrin, Flotillin, RhoA, and Cdc42 (a biomarker of macropinocytosis). The results of this experiment on colocalization and endocytosis pathway inhibitors demonstrated that AM-PEG NSs probably enter MCF-7 cells through macropinocytosis and caveolin-dependent pathways rather than pathways dependent on clathrin, Flotillin, Arf6, RhoA, or Cdc42 (Figure 2a–d and Figures S11–S15, Supporting Information). As reported for the classic endocytosis pathways, after being internalized into the cells, nanomaterials are transported to early endosomes, late endosomes, and lysosomes (in order). Rab5 is widely used as a marker of early endosomes and Rab7 as a marker of late endosomes, whereas lysosomal-associated membrane protein 1 (LAMP-1) is used to mark lysosomes. We then sought to verify whether these AM-PEG NSs are transported through this pathway by detecting colocalization. As illustrated in Figure 2e–g, red fluorescent AM-PEG NSs colocalized perfectly with early and late endosomes (EGFP-labeled Rab5 and Rab7) and LAMP-1-marked lysosomes. In addition, semiquantiative statistical analysis of Pearson's correlation coefficient was used to further examine colocalization by extracting the intensity of each color in these images (Figure S16, Supporting Information). The Rr ranged from 0.744 to 0.884, indicating good linear relationships between pairs of colors and good colocalization between different markers. The Pearson's correlation coefficient is consistent with our confocal images. It can be concluded from the results that AM-PEG NSs were taken up by MCF-7 cells through macropinocytosis and caveolin-dependent endocytosis pathways, then transported via "early endosomes"–"late endosomes"–"lysosomes" through the classic endocytosis pathways, as summarized in Figure 2h. We expect these clarifications regarding the detailed molecular mechanisms and kinetic pathways to help pave the way for their safe and efficient biomedical application, such as novel therapeutic strategies related to these pathways.[22b–d] In addition, some overlooked factors at the nano–bio interface (e.g., cell sex, cell passage number, cell source, etc.) that may accelerate clinical translation of such nanotechnologies should also be noted.[33]

As has been well recognized, the design of nanomedicines for cancer therapy must take into account a series of biological processes[22a,34] that includes blood circulation, vessel extravasation, and tumor site accumulation, as well as deep penetration into tumor and tumor cell uptake before therapeutics are released. Although nanoplatforms around 100 nm in size have the advantages of superior pharmacokinetics and vascular extravasation,[35] they are ill-suited to deep tumor penetration because of the barrier formed by the interstitial tumor matrix and huge diffusional hindrance. Conversely, smaller nanoplatforms are preferred for tumor penetration[36] but are rapidly cleared during blood circulation, leading to insufficient tumor accumulation.[37] For these reasons more attention has been paid to "intelligent" size shrinkable (or multistage) nanoplatforms.[38] However, compared with size-shrinkable nanoplatforms whose design is complicated, the simply designed AM-PEG/DOX NSs might offer an promising alternative strategy for conquering the penetration problem: after these NSs arrive at the tumor site, release of the loaded drugs will be triggered by the NIR laser and pH, and the released small molecules will be perfectly fit for high tumor penetration compared with nanoplatforms. To verify these assumptions, we evaluated the photo-induced

penetrating ability of AM-PEG/DOX NSs in MCF-7 tumor spheroids. As illustrated in Figure 3a–c, after only 5 min of irradiation (0.8 W cm^{-2}) and 3 h of further incubation, strong fluorescence signals could be detected from the periphery to the center of the tumor spheroids via confocal laser scanning microscopy (CLSM) images. In contrast, only the outer ring of the tumor spheroid showed fluorescence signals, and much less signal was detected within the spheroids (especially the central part) in the group without (W/O)-laser irradiation compared with the irradiation group. Quantitative analysis of the fluorescence intensity within the four middle slices of the tumor spheroids in both groups further confirmed the superiority of this photo-induced, enhanced tumor-penetration strategy for AM-PEG/DOX NSs (Figure S17, Supporting Information).

Having confirmed the benefit of high tumor penetration, we moved on to explore the possibility of enhanced cell uptake of AM-PEG/DOX NSs via the mild photothermal effect produced by irradiation. As shown in Figure 3d, flow cytometry (FCM) profiles revealed that mild photothermal heating enhanced the intracellular uptake of AM-PEG/DOX NSs, as the fluorescence was stronger in the laser irradiation group (0.5 W cm^{-2}, 10 min) than in the control group (without laser irradiation). The final temperature stage in the laser irradiation group was 43.3–43.7 °C for 5 min (Figure 3e), while the temperature in the control group remained 37 °C for the whole period. The enhanced cell uptake could be attributed to the photo-induced local heating of cytomembrane associated with AM-PEG/DOX NSs, which greatly increases the permeability of the membrane.[39] We then investigated the in vitro combined therapeutic effects of these NSs. MCF-7 cells were incubated with free DOX, AM-PEG NSs, or AM-PEG/DOX NSs with or without NIR irradiation (808 nm, 0.8 W cm^{-2}, 5 min). As shown in Figure 3f, no toxicity was observed in the groups treated with NIR alone or AM-PEG NSs alone. Among MCF-7 cells treated with AM-PEG/DOX NSs, 37.4% were killed, fewer than by free DOX (43.7%). The cytotoxicity among MCF-7 cells treated with both AM-PEG NSs and NIR irradiation (PTT group) was slightly higher than the chemotherapy groups (i.e., DOX and AM-PEG/DOX NSs) at the tested conditions. When the AM-PEG NSs were combined with both DOX loading and NIR laser irradiation, almost all of the MCF-7 cells were killed (91.5%), indicating a dramatic therapeutic effect. Similar results were obtained with PC3 cells (Figure S18, Supporting Information), demonstrating the high efficacy of combined chemophotothermal therapy strategy based on AM-PEG/DOX NSs.

Spurred on by these exciting in vitro results, we designed a final set of experiments including in vivo animal assays to explore the potential of AM-PEG/DOX NSs as effective photo nic nanomedicines for cancer theranostics. The biodistribution and tumor accumulation of the developed AM-based delivery platform were assessed by in vivo fluorescence imaging using Cy5.5-labeled AM-PEG NSs. As shown in Figure 4a, considerable fluorescence signals were detected in the tumor sites 2 h after intravenous (i.v.) injection: the subcutaneous tumor could be clearly distinguished from other tissues. In addition, the fluorescence signals of the tumor sites gradually increased with time, indicating that these NSs continued to accumulate. Meanwhile, at 24 h post-injection, the fluorescence signals at the tumor sites remained very strong, suggesting good accumulation and retention of the NSs via blood circulation and the enhanced permeability and retention (EPR) effect. We further demonstrated the superior tumor accumulation and retention of Cy5.5-labeled

AM-PEG NSs through ex vivo study of excised tumor and organs 24 h after injection (Figure 4b). Strong fluorescence signals were detected mainly in the tumor and in organs such as liver, lung, and kidney. Accumulation of NSs in the liver could be attributed to absorption by the reticuloendothelial system, which in the kidney may be caused by possible renal excretion, and which in the lung may be related to mechanical retention of large-sized NSs. Nevertheless, dense accumulation of NSs in the tumor (Figure 4c) was due to the EPR effect, indicating promise for systematic delivery in cancer treatment. In addition, the extended circulation time verified through pharmacokinetic studies was also in good agreement with the biodistribution results (Figure S19, Supporting Information).

Due to benefits such as reducing unnecessary biopsies and facilitating imaging-guided cancer theranostics, noninvasive imaging has attracted considerable research interest.[40] PA imaging is among the most promising biophotonic diagnostic modalities, in multiple ways superior to many other traditional optical imaging techniques.[41] Advantages of PA imaging include deep penetration (up to several centimeters), depth-resolved 3D imaging, superior sensitivity, high spatial resolution, and molecule-specific image contrast. To evaluate the in vivo PA performance of the developed AM-based delivery platforms, we compared them to BP-based nanomaterials, which are now among the most-popular 2D materials and have been extensively studied as promising drug-delivery platforms and PA agents for cancer theranostics.[18a,42] BP-PEG NSs (with similar size, thickness, and shape) were developed according to our previous report.[18a] As shown in Figure 4d, much stronger PA signals were observed at the tumor sites 12 h after i.v. injection of AM-PEG NSs through in vivo ultrasound and PA images at both 780 and 808 nm wavelengths, compared to BP-PEG NSs at the same dose and condition. In addition, the quantitative analysis of each ROI signal by ImageJ further demonstrated that the PA performance of the developed AM-based delivery platforms were superior to those of BP platforms (Figure 4e). After confirming the potential PA application of the AM-based delivery platforms, we continued to demonstrate their enhanced penetration ability under NIR irradiation using Cy5.5-loaded AM-PEG NSs. As can be seen in the ex vivo tumor slices (Figure 4f and g), nearly all the fluorescent molecules loaded on the NSs were in the tumor vessels, and very few were detected in the extravascular tumor parenchyma in tumors without NIR irradiation. However, a large amount of fluorescence signal spread from tumor vessels and highly concentrated within the tumor sections taken from the NIR irradiation group, clearly demonstrating the deep tumor penetration of the loaded molecules produced by the combination of NIR laser treatment and the acid TME. This photo-induced, pH-enhanced tumor-penetration strategy could further enhance the in vivo antitumor efficacy of the developed AM-based delivery platforms.

To validate the potential antitumor efficacy of AM-PEG/DOX NSs in vivo, MCF-7 breast tumor models were established and antitumor studies were carried out in Balb/c nude mice. The mice were treated as follows. Group 1: saline, Group 2: DOX, Group 3: AM-PEG/DOX NSs, Group 4: AM-PEG NSs + NIR, and Group 5: AM-PEG/DOX NSs. The i.v.-injected doses of DOX and AM-PEG NSs were both 6 mg kg^{-1} in all relevant groups. Groups 4 and 5 were irradiated with NIR laser (0.8 W cm^{-2}, 808 nm) for 10 min 12 h post-injection. An IR thermal camera was used to record the temperature changes in different groups via photothermal imaging (Figure 5a,b). Under 10 min of NIR irradiation, the tumor temperatures of mice i.v. injected with AM-PEG or AM-PEG/DOX NSs significantly

increased to ≈52 °C, while the temperatures in Groups 1–3 without NIR irradiation treatment remained stable (≈33–34 °C). After different treatments, the volumes of tumors were calculated on the basis of their length and width measured by a digital caliper every 2 d (Figure 5c). As expected, Groups 2–5 all showed different levels of tumor growth inhibition (TGI) compared to the control group injected with saline (Figure S20, Supporting Information). Better therapeutic effects were found in Groups 3 (TGI rate of 55.4%) and 4 (TGI rate of 73.1%) than in Group 2 (free commercial chemotherapy drugs, TGI rate of 43.6%). Notably, Group 5 showed extremely high inhibition of tumor growth (TGI rate of 98.1%), indicating the remarkably enhanced therapeutic effect of chemophotothermal combined treatment compared with single chemotherapy or single PTT. In addition, the antitumor effect in Group 5 is calculated to be an efficient synergistic effect of chemotherapy and PTT according to well-demonstrated methods, rather than a simple additive effect (see Supporting Information). Digital photos of tumors excised from representative mice also reflect the excellent therapeutic effect of the AM-PEG/DOX NSs (Figure 5d). The very positive therapeutic effect in Group 5 was achieved by only a single treatment on Day 0, rather than the continuous treatment in Groups 1–3 (Figure S21, Supporting Information). None of the treatment groups demonstrated any obvious side effects, such as abnormal weight loss (Figure S22, Supporting Information), pathological changes (Figure 5e), neurological issues, or perturbations in eating, drinking, or activity. In addition, we further provided the results based on intratumorally (*i.t.*) injection of the therapeutics to further explore the therapeutic efficacy. As shown in Figure S23 in the Supporting Information, even using a half-dose of the AM nanomaterials (1 mg kg^{-1}) and a lower power density (0.8 W cm^{-2}) compared to our previous report,[17] the chemophotothermal combined therapy group (Group 5) still displayed complete elimination of tumors, indicating more significant potential of applying such NSs to cancer treatment.

Having confirmed the excellent in vivo performance of these multimodal-imaging-guided cancer theranostics, we finally examined preliminary biosafety and metabolic degradation of these NSs. As shown in Figure S24 in the Supporting Information, results of complete blood parameter analysis after i.v. injection of AM-based NSs were within normal ranges, suggesting likely biosafety. Moreover, a series of experiments preliminarily accessed the metabolic degradation of AM-based NSs using previously reported methods.[18d] As shown in Figure S25a–c in the Supporting Information, the photothermal effects and UV/vis–NIR absorbance spectra gradually receded during the three heating–cooling cycles in water under the irradiation of an 808 nm NIR laser. In the meantime, the black color of both AM NSs faded until becoming nearly transparent during the irradiation cycles, indicating the possible degradation of AM NSs in water. However, the photothermal effects and UV/vis–NIR absorbance remained constant in the exfoliation solution (ethanol) as seen in Figure S25d–f in the Supporting Information, suggesting that water may be necessary for the degradation of AM NSs. We further incubated the developed AM NSs in water for different numbers of days in an oxygen atmosphere (Figure S25g–i) or in an oxygen-free environment (Figure S25j–l), and the photothermal effects and UV/vis–NIR absorbance spectra were tested using similar methods. The presence of oxygen strongly accelerated degradation in water, indicating that the underlying mechanism might be oxidative degradation of AM NSs. In order to confirm the metabolism of AM-based NSs in vivo (i.e., retention versus clearance/

degradation), we further performed a long-term biodistribution study using inductively coupled plasma mass spectrometric analysis of antimony in different organs. As displayed in Figure S26 in the Supporting Information, antimony levels in the major organs showed a distinct trend of persistent decrease, and AM-based NSs were barely detectable 30 d after i.v. injection, indicating the clearance of these NSs from the mouse body, which might represent fully metabolic degradation. The potential degradability of these AM-based NSs makes them quite promising for applications in cancer theranostics. However, more systematic in vivo studies are still needed before clinical studies of these PEGylated AM-based NSs. Further discussion is provided in the Supporting Information.

In conclusion, we present the first report of the promising application of AM-PEG NSs as photonic drug-delivery platforms for cancer theranostics. Using DOX as a model drug, AM-PEG NSs showed high drug loading capacity and multiresponsive (i.e., pH-/photoresponsive) release properties after either extrinsic or intrinsic stimuli, and were much simpler in design. The nanobio interactions of AM-PEG NSs within MCF-7 cells were revealed for the first time, providing an essential understanding and useful references for AM or other extensively studied 2D nanomaterials for cancer theranostics. Additional photo-induced benefits of AM-PEG/DOX NSs such as high cellular uptake and deep tumor penetration were also confirmed. Significant positive outcomes were obtained after antitumor therapy guided by multimodal imaging (fluorescence/PA/photothermal imaging) both in vitro and in vivo with AM-PEG/DOX NSs. With excellent biocompatibility, potential degradability, and clinical applications of antimonial drugs, the developed AM-based delivery platforms hold great promise for cancer theranostics. More comprehensive studies of this novel 2D nanomaterial may be inspired by this work, similar to those carried out with graphene, MoS_2, and BP.

Supplementary Material

Refer to Web version on PubMed Central for supplementary material.

Acknowledgements

W.T., X.J., and X.Z. contributed equally to this work. We thank Prof. Jinjun Shi from Harvard Medical School for helpful discussions. For their constructive suggestions and editorial contributions we are grateful to Dr. Xiaoding Xu, Dr. Mikyung Yu, Dr. Jianxun Ding, Austin Barrett from Harvard Medical School, and Jinxie Zhang and Dr. Xudong Zhang from Tsinghua University. This study was supported by grants from the US National Institutes of Health (NIH) HL127464, David H. Koch-Prostate Cancer Foundation (PCF) Program in Cancer Nanotherapeutics, National Research Foundation of Korea grant K1A1A2048701, Natural Science Foundation of Guangdong Province 2016A030310023, China Postdoctoral Science Foundation 2016M600676, and Tsinghua Scholarship for Overseas Graduate Studies 2013159. All in vivo studies were performed in accordance with National Institutes of Health animal care guidelines and in strict pathogen-free conditions in the animal facilities of Brigham and Women's Hospital. The animal protocol was approved by the Institutional Animal Care and Use Committees at Harvard Medical School.

References

[1]. a)Novoselov KS, Geim AK, Morozov SV, Jiang D, Zhang Y, Dubonos SV, Grigorieva IV, Firsov AA, Science 2004, 306, 666; [PubMed: 15499015] b)Zhang Y, Tang T-T, Girit C, Hao Z, Martin MC, Zettl A, Crommie MF, Shen YR, Wang F, Nature 2009, 459, 820; [PubMed: 19516337] c)Novoselov KS, Falko VI, Colombo L, Gellert PR, Schwab MG, Kim K, Nature 2012, 490, 192. [PubMed: 23060189]

[2]. a)Geim AK, Science 2009, 324, 1530; [PubMed: 19541989] b)Peng X, Peng L, Wu C, Xie Y, Chem. Soc. Rev 2014, 43, 3303; [PubMed: 24614864] c)Li X, Zhu J, Wei B, Chem. Soc. Rev 2016;d)Chhowalla M, Shin HS, Eda G, Li L-J, Loh KP, Zhang H, Nat. Chem 2013, 5, 263. [PubMed: 23511414]

[3]. Fiori G, Bonaccorso F, Iannaccone G, Palacios T, Neumaier D, Seabaugh A, Banerjee SK, Colombo L, Nat. Nanotechnol 2014, 9, 768. [PubMed: 25286272]

[4]. Wang QH, Kalantar-Zadeh K, Kis A, Coleman JN, Strano MS, Nat. Nanotechnol 2012, 7, 699. [PubMed: 23132225]

[5]. Liu C, Kong D, Hsu P-C, Yuan H, Lee H-W, Liu Y, Wang H, Wang S, Yan K, Lin D, Maraccini PA, Parker KM, Boehm AB, Cui Y, Nat. Nanotechnol 2016, 11, 1098. [PubMed: 27525474]

[6]. Deng D, Novoselov KS, Fu Q, Zheng N, Tian Z, Bao X, Nat. Nanotechnol 2016, 11, 218. [PubMed: 26936816]

[7]. Chen Y, Tan C, Zhang H, Wang L, Chem. Soc. Rev 2015, 44, 2681. [PubMed: 25519856]

[8]. Cao X, Tan C, Zhang X, Zhao W, Zhang H, Adv. Mater 2016, 28, 6167. [PubMed: 27071683]

[9]. Mannix AJ, Kiraly B, Hersam MC, Guisinger NP, Nat. Rev. Chem 2017, 1, 0014.

[10]. Mannix AJ, Zhou X-F, Kiraly B, Wood JD, Alducin D, Myers BD, Liu X, Fisher BL, Santiago U, Guest JR, Yacaman MJ, Ponce A, Oganov AR, Hersam MC, Guisinger NP, Science 2015, 350, 1513. [PubMed: 26680195]

[11]. a)Vogt P, De Padova P, Quaresima C, Avila J, Frantzeskakis E, Asensio MC, Resta A, Ealet B, Le Lay G, Phys. Rev. Lett 2012, 108, 155501; [PubMed: 22587265] b)Amlaki T, Bokdam M, Kelly PJ, Phys. Rev. Lett 2016, 116, 256805. [PubMed: 27391742]

[12]. Li L, Yu Y, Ye GJ, Ge Q, Ou X, Wu H, Feng D, Chen XH, Zhang Y, Nat. Nanotechnol 2014, 9, 372. [PubMed: 24584274]

[13]. Zhang S, Xie M, Li F, Yan Z, Li Y, Kan E, Liu W, Chen Z, Zeng H, Angew. Chem. Int. Ed 2016, 128, 1698.

[14]. Wang G, Pandey R, Karna SP, ACS Appl. Mater. Interfaces 2015, 7, 11490. [PubMed: 25955131]

[15]. a)Lee J, Tian W-C, Wang W-L, Yao D-X, Sci. Rep 2015, 5, 11512; [PubMed: 26122870] b)Ji J, Song X, Liu J, Yan Z, Huo C, Zhang S, Su M, Liao L, Wang W, Ni Z, Hao Y, Zeng H, Nat. Commun 2016, 7, 13352. [PubMed: 27845327]

[16]. a)Gibaja C, Rodriguez-San-Miguel D, Ares P, Gomez-Herrero J, Varela M, Gillen R, Maultzsch J, Hauke F, Hirsch A, Abellan G, Zamora F, Angew. Chem. Int. Ed 2016, 55, 14345;b)Ares P, Aguilar-Galindo F, Rodriguez-San-Miguel D, Aldave DA, Diaz-Tendero S, Alcami M, Martin F, Gomez-Herrero J, Zamora F, Adv. Mater 2016, 28, 6332. [PubMed: 27272099]

[17]. Tao W, Ji X, Xu X, Islam MA, Li Z, Chen S, Saw PE, Zhang H, Bharwani Z, Guo Z, Shi J, Farokhzad OC, Angew. Chem. Int. Ed 2017, 56, 11896.

[18]. a)Tao W, Zhu X, Yu X, Zeng X, Xiao Q, Zhang X, Ji X, Wang X, Shi J, Zhang H, Mei L, Adv. Mater 2017, 29, 1603276;b)Yang K, Feng L, Shi X, Liu Z, Chem. Soc. Rev 2013, 42, 530; [PubMed: 23059655] c)Wang S, Chen Y, Li X, Gao W, Zhang L, Liu J, Zheng Y, Chen H, Shi J, Adv. Mater 2015, 27, 7117; [PubMed: 26447460] d)Shao J, Xie H, Huang H, Li Z, Sun Z, Xu Y, Xiao Q, Yu XF, Zhao Y, Zhang H, Wang H, Chu PK, Nat. Commun 2016, 7, 12967; [PubMed: 27686999] e)Jiang T, Sun W, Zhu Q, Burns NA, Khan SA, Mo R, Gu Z, Adv. Mater 2015, 27, 1021. [PubMed: 25504623]

[19]. Chimene D, Alge DL, Gaharwar AK, Adv. Mater 2015, 27, 7261. [PubMed: 26459239]

[20]. Zhang S, Yan Z, Li Y, Chen Z, Zeng H, Angew. Chem. Int. Ed 2015, 54, 3112.

[21]. a)Frezard F, Demicheli C, Ribeiro RR, Molecules 2009, 14, 2317; [PubMed: 19633606] b)Kuryshev YA, Wang L, Wible BA, Wan X, Ficker E, Mol. Pharmacol 2006, 69, 1216. [PubMed: 16418337]

[22]. a)Shi J, Kantoff PW, Wooster R, Farokhzad OC, Nat. Rev. Cancer 2017, 17, 20; [PubMed: 27834398] b)Zhu X, Ji X, Kong N Chen Y, Mahmoudi M, Xu X, Ding L, Tao W, Cai T, Li Y, Gan T, Barrett A, Bharwani Z, Chen H, Farokhzad OC, ACS Nano 2018, 12, 2922; [PubMed: 29406760] c)Ding L, Zhu X, Wang Y, Shi B, Ling X, Chen H, Nan W, Barrett A, Guo Z, Tao W, Wu J, Shi X, Nano Lett 2017, 17, 6790; [PubMed: 29058908] d)Behzadi S, Serpooshan V, Tao W, Hamaly MA, Alkawareek MY, Dreaden EC, Brown D, Alkilany AM, Farokhzad OC, Mahmoudi M, Chem. Soc. Rev 2017, 46, 4218. [PubMed: 28585944]

[23]. Lannin JS, Calleja JM, Cardona M, Phys. Rev. B 1975, 12, 585.

[24]. Liu H, Neal AT, Zhu Z, Luo Z, Xu X, Tománek D, Ye PD, ACS Nano 2014, 8, 4033. [PubMed: 24655084]

[25]. a)Sun Z, Xie H, Tang S, Yu X-F, Guo Z, Shao J, Zhang H, Huang H, Wang H, Chu PK, Angew. Chem. Int. Ed 2015, 3, 11526;b)Lu W, Xiong C, Zhang G, Huang Q, Zhang R, Zhang JZ, Li C, Clin. Cancer Res 2009, 15, 876. [PubMed: 19188158]

[26]. Liu T, Wang C, Gu X, Gong H, Cheng L, Shi X, Feng L, Sun B, Liu Z, Adv. Mater 2014, 26, 3433. [PubMed: 24677423]

[27]. Sun X, Liu Z, Welsher K, Robinson JT, Goodwin A, Zaric S, Dai H, Nano Res 2008, 1, 203. [PubMed: 20216934]

[28]. a)Tao W, Zeng X, Wu J, Zhu X, Yu X, Zhang X, Zhang J, Liu G, Mei L, Theranostics 2016, 6, 470; [PubMed: 26941841] b)Tao W, Zeng X, Liu T, Wang Z, Xiong Q, Ouyang C, Huang L, Mei L, Acta Biomater 2013, 9, 8910; [PubMed: 23816645] c)Tao W, Zhang J, Zeng X, Liu D, Liu G, Zhu X, Liu Y, Yu Q, Huang L, Mei L, Adv. Healthcare Mater 2015, 4, 1203;d)Tao W, Zeng X, Zhang J, Zhu H, Chang D, Zhang X, Gao Y, Tang J, Huang L, Mei L, Biomater. Sci 2014, 2, 1262.

[29]. Lu Y, Aimetti AA, Langer R, Gu Z, Nat. Rev. Mater 2016, 2, 16075.

[30]. Rosenblum D, Joshi N, Tao W, Karp JM, Dan P, Nat. Commun 2018, 9, 1410. [PubMed: 29650952]

[31]. Conner SD, Schmid SL, Nature 2003, 422, 37. [PubMed: 12621426]

[32]. Mayor S, Pagano RE, Nat. Rev. Mol. Cell Biol 2007, 8, 603. [PubMed: 17609668]

[33]. a)Mahmoudi M, Trends Biotechnol, 2018, 10.1016/j.tibtech.2018.02.014;b)Serpooshan V, Sheibani S, Pushparaj P, Wojcik M, Jang AY, Santoso MR, Jang JH, Huang H, Safavi-Sohi R, Haghjoo N, Nejadnik H, Aghaverdi H, Vali H, Kinsella JM, Presley J, Xu K, Yang PC-M, Mahmoudi M, ACS Nano 2018, 12, 2253. [PubMed: 29536733]

[34]. a)Godin B, Tasciotti E, Liu X, Serda RE, Ferrari M, Acc. Chem. Res 2011, 44, 979; [PubMed: 21902173] b)Sanhai WR, Sakamoto JH, Canady R, Ferrari M, Nat. Nanotechnol 2008, 3, 242; [PubMed: 18654511] c)Lee Y, Lee S, Lee DY, Yu B, Miao W, Jon S, Angew. Chem. Int. Ed 2016, 55, 10676;d)Gao W, Zhang L, J. Drug Target 2015, 23, 619. [PubMed: 26453159]

[35]. Perrault SD, Walkey C, Jennings T, Fischer HC, Chan WCW, Nano Lett 2009, 9, 1909. [PubMed: 19344179]

[36]. a)Cabral H, Matsumoto Y, Mizuno K, Chen Q, Murakami M, Kimura M, Terada Y, Kano MR, Miyazono K, Uesaka M, Nishiyama N, Kataoka K, Nat. Nanotechnol 2011, 6, 815; [PubMed: 22020122] b)Chauhan VP, Stylianopoulos T, Martin JD, Popovic Z, Chen O, Kamoun WS, Bawendi MG, Fukumura D, Jain RK, Nat. Nanotechnol 2012, 7, 383. [PubMed: 22484912]

[37]. a)Soo Choi H, Liu W, Misra P, Tanaka E, Zimmer JP, Itty Ipe B, Bawendi MG, Frangioni JV, Nat. Biotechnol 2007, 25, 1165; [PubMed: 17891134] b)Choi HS, Liu W, Liu F, Nasr K, Misra P, Bawendi MG, Frangioni JV, Nat. Nanotechnol 2010, 5, 42. [PubMed: 19893516]

[38]. a)Li H-J, Du J-Z, Du X-J, Xu C-F, Sun C-Y, Wang H-X, Cao Z-T, Yang X-Z, Zhu Y-H, Nie S, Wang J, Proc. Natl. Acad. Sci. USA 2016, 113, 4164; [PubMed: 27035960] b)Sun Q, Sun X, Ma X, Zhou Z, Jin E, Zhang B, Shen Y, Van Kirk EA, Murdoch WJ, Lott JR, Lodge TP, Radosz M, Zhao Y, Adv. Mater 2014, 26, 7615; [PubMed: 25328159] c)Tong R, Chiang HH, Kohane DS, Proc. Natl. Acad. Sci. USA 2013, 110, 19048; [PubMed: 24191048] d)Wong C, Stylianopoulos T, Cui J, Martin J, Chauhan VP, Jiang W, Popović Z, Jain RK, Bawendi MG, Fukumura D, Proc. Natl. Acad. Sci. USA 2011, 108, 2426. [PubMed: 21245339]

[39]. a)Sherlock SP, Tabakman SM, Xie L, Dai H, ACS Nano 2011, 5, 1505; [PubMed: 21284398] b)Kim J, Kim J, Jeong C, Kim WJ, Adv. Drug Deliver. Rev 2016, 98, 99.

[40]. a)Ni D, Jiang D, Valdovinos HF, Ehlerding EB, Yu B, Barnhart TE, Huang P, Cai W, Nano Lett 2017, 17, 3282; [PubMed: 28418679] b)Kunjachan S, Ehling J, Storm G, Kiessling F, Lammers T, Chem. Rev 2015, 115, 10907; [PubMed: 26166537] c)Ni D, Zhang J, Wang J, Hu P, Jin Y, Tang Z, Yao Z, Bu W, Shi J, ACS Nano 2017, 11, 4256; [PubMed: 28323405] d)Ni D, Bu W, Ehlerding EB, Cai W, Shi J, Chem. Soc. Rev 2017, 46, 7438; [PubMed: 29071327] e)Ni D, Jiang D, Ehlerding EB, Huang P, Cai W, Acc. Chem. Res 2018, 51, 778. [PubMed: 29489335]

[41]. Wang LV, Hu S, Science 2012, 335, 1458. [PubMed: 22442475]

[42]. Sun Z, Zhao Y, Li Z, Cui H, Zhou Y, Li W, Tao W, Zhang H, Wang H, Chu PK, Yu X-F, Small 2017, 13, 1602896.

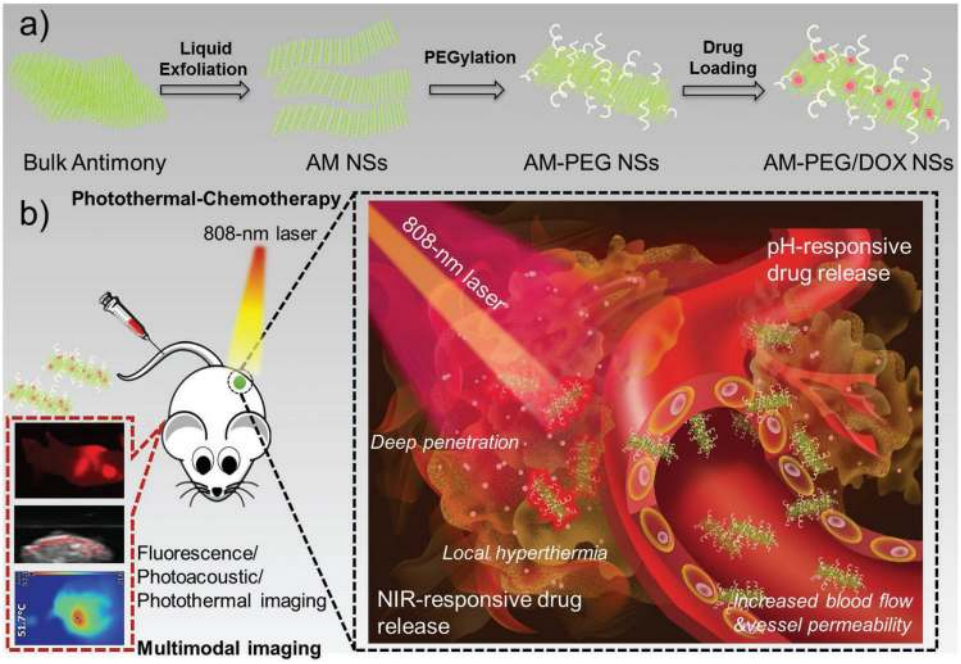

Scheme 1.

Schematic illustrations of: a) the preparation of 2D AM-PEG/DOX NSs; and b) the systemic administration of AM-PEG/DOX NSs as photonic nanomedicines for multimodal-imaging-guided cancer theranostiocs.

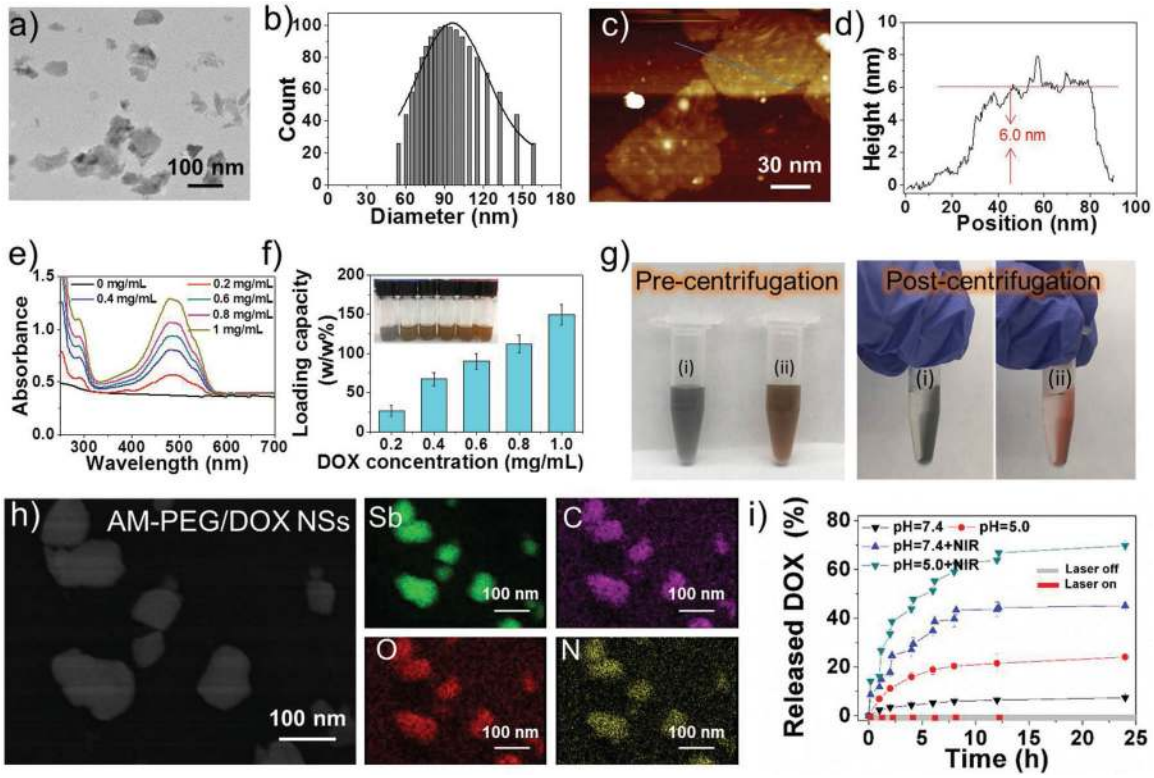

Figure 1.

Characterization of the AM-based NSs. a) TEM image, b) size distribution, c) AFM image, and d) thickness measured from (c) of the 2D AM-PEG NSs. e) UV–vis–NIR absorbance of AM-PEG/DOX NSs at different DOX feeding concentrations after the removal of excess-free DOX. f) DOX loading capacities on AM-PEG NSs (w/w%) with increasing DOX feeding concentrations. g) Photographs of (i) AM-PEG NSs and (ii) AM-PEG/DOX NSs solution before and after centrifugation. h) STEM-EDC mapping images of AM-PEG/DOX NSs. i) Release profiles of DOX at different pHs with or without 808-nm NIR laser (0.8 W cm^{-2}).

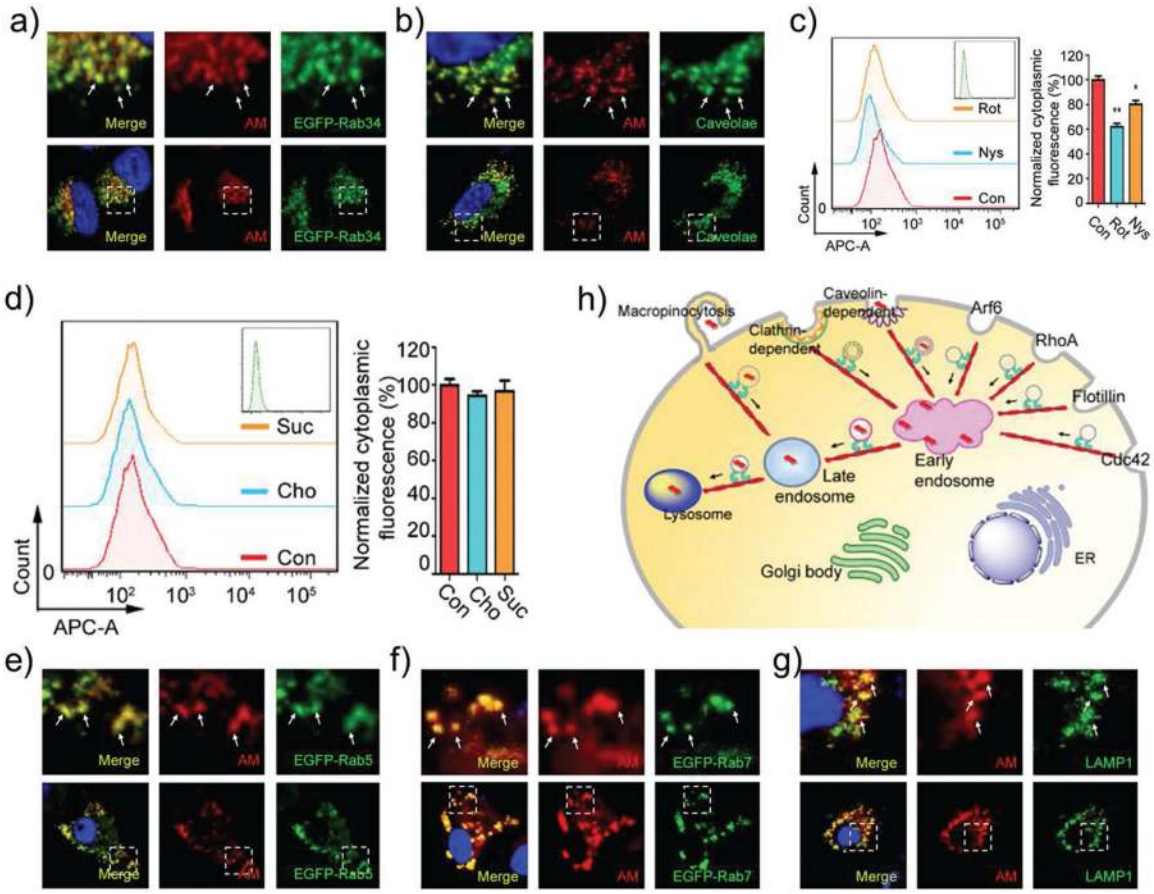

Figure 2.

Intracellular fate of AM-PEG NSs. The Cy5.5-labeled AM-PEG NSs enter MCF-7 cells through: a) Macropinocytosis and b) Caveolin-dependent endocytosis. Cytoplasmic fluorescence measured by FCM of cells pretreated with: c) micropinocytosis pathway inhibitor (Rot) and Caveolin-dependent pathway inhibitor (Nys), and d) Clathrin-dependent pathway inhibitors (Cho and Suc) for 2 h. After endocytosis, the AM-PEG NSs are transported by: e) early endosomes, f) late endosomes, and finally into: g) lysosome. h) Schematic representation of how FITC-labeled AM-PEG NSs enter and travel in the MCF-7 cells (scale bars: 10 μm).

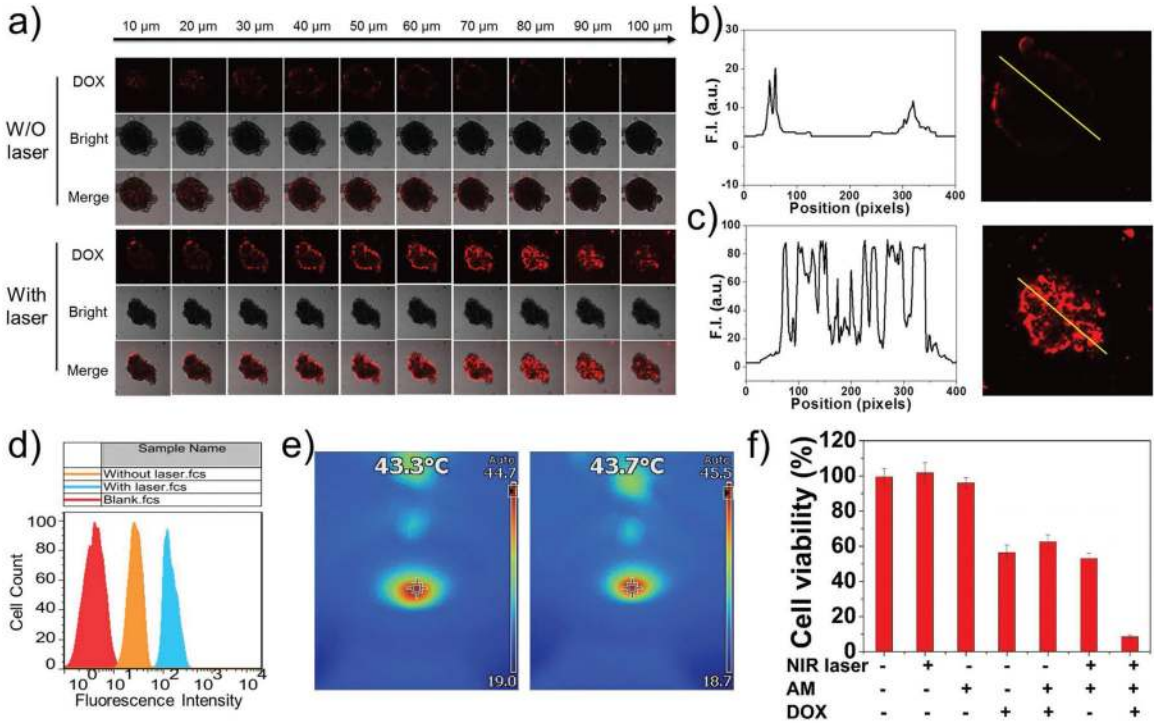

Figure 3.

Photo-induced benefits and in vitro combined cancer therapy. a) CLSM images of MCF-7 3D multicellular tumor spheroids after incubation with AM-PEG/DOX NSs for 3 h without (W/O) or with pre-treatment of 808-nm laser irradiation. Z-stack images were obtained from the top toward the tumor spheroid equatorial plane at 10-μm intervals. b) Fluorescence intensity measured from the equatorial plane of tumor spheroid in the W/O laser group. c) Fluorescence intensity measured from the equatorial plane of tumor spheroid in the with laser group. d) FCM histogram profiles of cellular DOX fluorescence intensity in MCF-7 cells W/O or with laser irradiation. e) Thermal images of 96-well plate during laser irradiation at final stage. f) Cell viability of MCF-7 cells with different treatments.

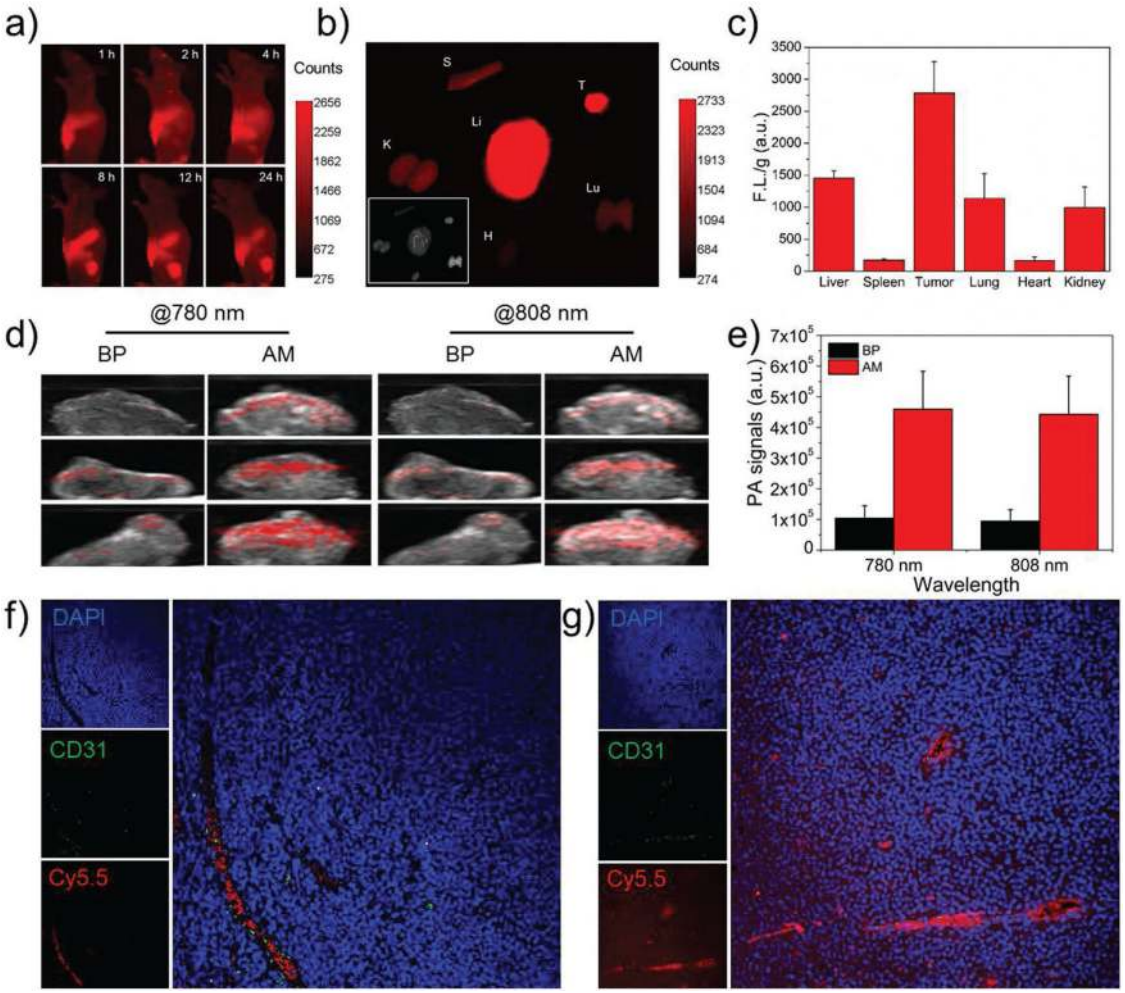

Figure 4.

In vivo multimodal imaging and penetration results of AM-based NSs. a) In vivo fluorescence images of nude mice at different time points after i.v. injection with Cy5.5-labeled AM-PEG NSs. b) Ex vivo fluorescence images of the tumor and major organs at 24 h post-injection. Li: Liver; S: Spleen; T: Tumor; Lu: Lung; H: Heart; and K: Kidney. c) Semiquantitative biodistribution of Cy5.5-labeled AM-PEG NSs in nude mice detected by the average fluorescence intensity of tumors and major organs per gram. d) In vivo ultrasound and PA images of tumors after i.v. injection with AM-PEG NSs at wavelengths of 780 and 808 nm. BP-PEG NSs at the same dose (3 mg kg^{-1}) were chosen as references. e) Quantitative analysis of each ROI signal in (d). Fluorescence images of the tumor sections of the MCF-7-tumor-bearing mouse sacrificed at 4 h post-injection of Cy5.5-loaded AM-PEG NSs: f) without, or g) with the irradiation of an 808 nm NIR laser (0.8 W cm^{-2}, 10 min).

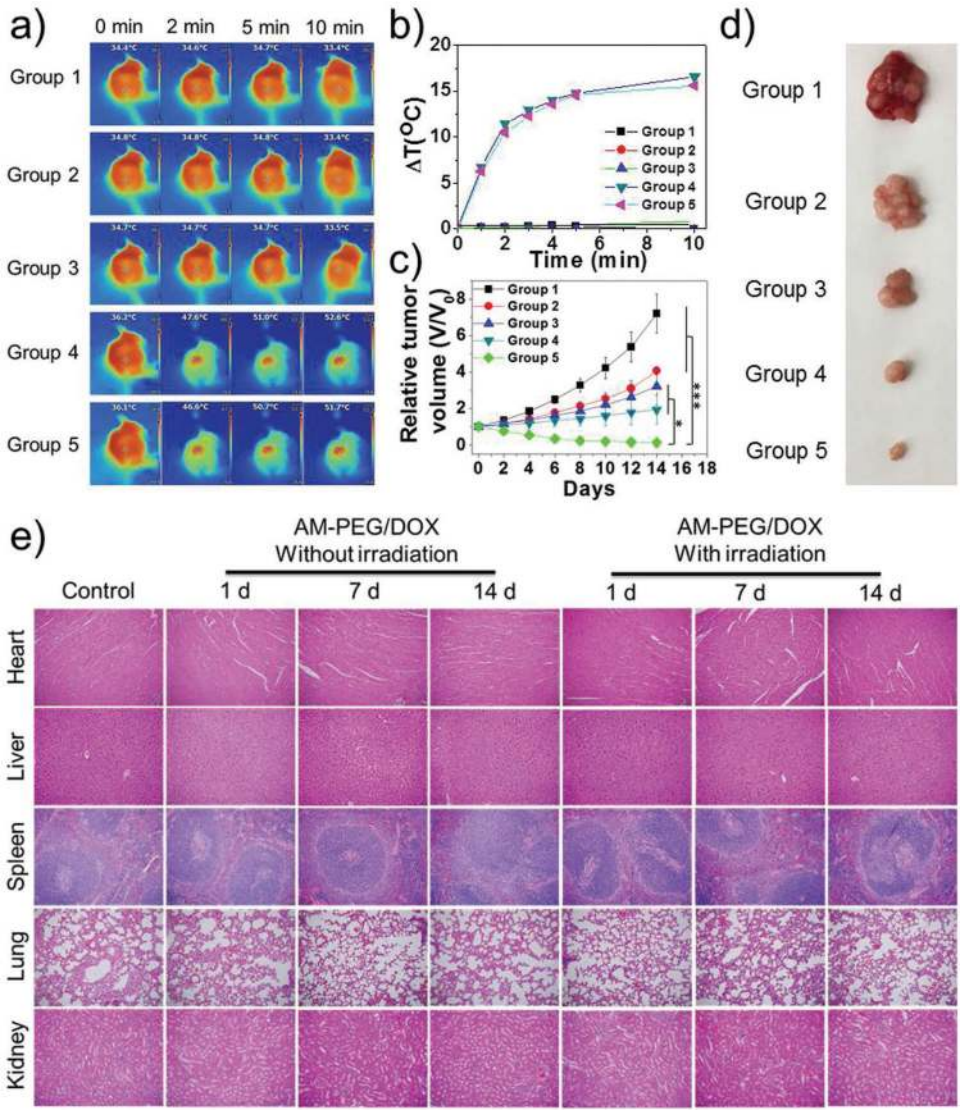

Figure 5.

In vivo combined cancer therapeutic effect of AM-based NSs. Group 1: saline; Group 2: DOX; Group 3: AM-PEG/DOX NSs; Group 4: AM-PEG NSs + NIR; and Group 5: AM-PEG/DOX NSs + NIR. NIR laser irradiation was performed in Groups 4 and 5 for 10 min (0.8 W cm^{-2}, 808 nm) after 12 h of i.v. injection ([AM] = 6 mg kg^{-1},[DOX] = 6 mg kg^{-1}). a) Infrared thermographic maps and b) time-dependent temperature changes in the MCF-7-tumor-bearing nude mice after different treatments. c) Growth curves of MCF-7-tumor-bearing nude mice after different treatments (*$P < 0.05$, ***$P < 0.001$). d) Digital photo of representative tumors in different groups after 14 d treatment. e) H&E-stained histological images of tissue sections from major organs (heart, liver, spleen, lung, and kidney) at 1, 7, and 14 d post-injection with different treatments.